Astron. Astrophys. 335, 488–499 (1998)

ASTRONOMY AND ASTROPHYSICS

Alpha-tensor and diffusivity tensor due to supernovae and superbubbles in the Galactic disk

Katia Ferrière

Observatoire Midi-Pyrénées, 14 Av. Ed. Belin, F-31400 Toulouse, France

Received 17 December 1997 / Accepted 16 March 1998

Abstract. Dynamo action (i.e., magnetic field amplification at large scales) requires the presence of turbulent motions, whose effects are traditionally described by the alpha- and diffusivity tensors. In the present paper, we compute the various components of these tensors, also known as the dynamo parameters, as a function of Galactic radius and height, on the hypothesis that the turbulent motions responsible for dynamo action in our Galaxy arise from supernova explosions. To that end, we combine ingredients taken from several earlier studies, including an up-to-date model of the interstellar medium, a numerical code designed to follow the expansion of supernova remnants and superbubbles in this model ISM, and analytical formulae for the dynamo parameters. Our computed dynamo parameters turn out to be predominantly due to clustered supernovae. They peak at about 7 kpc from the rotation axis and ~ 3 kpc from the midplane, reaching values in the expected range for magnetic field amplification.

Key words: Galaxy: general – ISM: bubbles; magnetic fields; supernova remnants

1. Introduction

The temporal evolution of the large-scale magnetic field in spiral galaxies is governed by the dynamo equation (Steenbeck, Krause, & Rädler 1966; Parker 1971; Vainshtein & Ruzmaikin 1971). According to this equation, the large-scale magnetic field is amplified through the combined effects of a large-scale velocity field and small-scale turbulent motions. The large-scale velocity field basically consists of the Galactic rotation and of a possible Galactic wind. The former is reasonably well established observationally, mainly thanks to HI and CO velocity measurements (e.g., Fich, Blitz, & Stark 1989). In contrast, the properties of turbulent motions are still poorly understood. It is commonly assumed that their impact on the large-scale magnetic field can be parameterized with the help of two tensors: the alpha-tensor, which represents the alpha-effect (generation of magnetic field perpendicular to the prevailing field) plus the net advection of field lines by turbulent motions, and the diffusivity tensor, which describes turbulent magnetic diffusion (e.g., Moffatt 1978).

For most calculations, each of these tensors is reduced to a single parameter, which ignores the anisotropic nature of the alpha-effect and of the turbulent magnetic diffusion as well as the net advection of field lines by turbulent motions. Furthermore, the diffusivity parameter is usually taken to be uniform throughout the Galactic disk, and while the alpha-parameter is often allowed to vary in space, its spatial dependence is chosen for mathematical convenience rather than on physical grounds. Finally, there exist only order-of-magnitude estimates for these parameters, founded, for instance, on mixing-length theory or on crude pictures of interstellar turbulence.

Our goal is to obtain realistic curves for all the components of the alpha- and diffusivity tensors throughout the Galaxy. We proceed from the assumption that turbulence in the interstellar medium (ISM) is driven by supernova (SN) explosions (McCray & Snow 1979), either isolated SNs which produce individual supernova remnants (SNRs) or clustered SNs which are responsible for the formation of superbubbles (SBs). We utilize the formal analytical expressions established by Ferrière (1993a) (hereafter Paper I) for the alpha-tensor and by Ferrière (1993b) (hereafter Paper II) for the diffusivity tensor due to an arbitrary distribution of axisymmetric explosions. These expressions are written in terms of the explosion rate, the large-scale rotation and shear rates, and the dynamical properties (lifetime, final shape. . .) of the shock wave driven by an explosion. We determine these properties with the help of the numerical code developed by Ferrière (1995) in order to follow the time evolution of SNRs and SBs in a prescribed ISM. The model ISM, in turn, is taken from Ferrière (1998). Note that the current paper constitutes a generalization of the study by Ferrière (1996) (hereafter Paper III) designed to compute the alpha- and diffusivity tensors in the vicinity of the Sun.

In Sect. 2, we review the main components of the model ISM. In Sect. 3, we explain how we model the expansion of SNRs and SBs. In Sect. 4, we provide formal expressions for the alpha- and diffusivity tensors. In Sect. 5, we present the numerical results and interpret them physically. In Sect. 6, we summarize our study and discuss its limitations.

Send offprint requests to: Katia Ferrière

2. Model interstellar medium

An axisymmetric model for the ISM was constructed by Ferrière (1998), based on the best-to-date observational data on the interstellar gas, cosmic rays, and magnetic fields, on the Galactic rotation curve and vertical gravitational acceleration, and on the parameters of the SN distribution. The available observational information, which contains several important gaps (mainly with regard to the hot gas component), was complemented with the requirement that the ISM be in hydrostatic equilibrium and with theoretical considerations on the radial dependence of the hot gas column density and scale height. It was thus fit into a comprehensive picture that represents, at best, the true ISM.

In this picture, the ISM is composed of a molecular medium, a cold neutral medium (CM), a warm neutral medium (WNM), a warm ionized medium (WIM), and a hot ionized medium (HM), respectively denoted by the subscripts m, c, w, i, and h. Hydrogen is completely neutral in the CM and in the WNM, while it is completely ionized in the WIM and in the HM. Helium, which represents 9% of hydrogen by number, is everywhere fully neutral except in the HM where it is doubly ionized.

The space-averaged number density of hydrogen nuclei in the different media is given as a function of Galactic radius, R, and height, Z, by

$$n_m(R,Z) = (0.58\ \mathrm{cm}^{-3}) \quad e^{-\frac{(R-4.5\ \mathrm{kpc})^2-(R_\odot-4.5\ \mathrm{kpc})^2}{(2.9\ \mathrm{kpc})^2}} \left(\frac{R}{R_\odot}\right)^{-0.58} e^{-\left(\frac{Z}{H_m(R)}\right)^2} , \quad (1)$$

with

$$H_m(R) = (81\ \mathrm{pc}) \left(\frac{R}{R_\odot}\right)^{0.58} ,$$

$$n_c(R,Z) = \frac{0.340\ \mathrm{cm}^{-3}}{h^2(R)} \left[0.859\, e^{-\left(\frac{Z}{H_1(R)}\right)^2} + 0.047\, e^{-\left(\frac{Z}{H_2(R)}\right)^2} + 0.094\, e^{-\frac{|Z|}{H_3(R)}}\right] , \quad (2)$$

$$n_w(R,Z) = \frac{0.226\ \mathrm{cm}^{-3}}{h(R)} \left[\left(1.745 - \frac{1.289}{h(R)}\right) e^{-\left(\frac{Z}{H_1(R)}\right)^2} + \left(0.473 - \frac{0.070}{h(R)}\right) e^{-\left(\frac{Z}{H_2(R)}\right)^2} + \left(0.283 - \frac{0.142}{h(R)}\right) e^{-\frac{|Z|}{H_3(R)}}\right] , \quad (3)$$

with

$$H_1(R) = (127\ \mathrm{pc})\, h(R) ,$$

$$H_2(R) = (318\ \mathrm{pc})\, h(R) ,$$

$$H_3(R) = (403\ \mathrm{pc})\, h(R) ,$$

$$h(R) = \begin{cases} 1 & 3.5\ \mathrm{kpc} \le R \le R_\odot \\ \dfrac{R}{R_\odot} & R_\odot \le R \le 20\ \mathrm{kpc} \end{cases} ,$$

$$n_i(R,Z) = (0.0237\ \mathrm{cm}^{-3})\ e^{-\frac{R^2-R_\odot^2}{(37\ \mathrm{kpc})^2}}\ e^{-\frac{|Z|}{1\ \mathrm{kpc}}} + (0.0013\ \mathrm{cm}^{-3})\ e^{-\frac{(R-4\ \mathrm{kpc})^2-(R_\odot-4\ \mathrm{kpc})^2}{(2\ \mathrm{kpc})^2}}\ e^{-\frac{|Z|}{150\ \mathrm{pc}}} , \quad (4)$$

and

$$n_h(R,Z) = \left(4.8\times10^{-4}\ \mathrm{cm}^{-3}\right) \left[0.12\, e^{-\frac{R-R_\odot}{4.9\ \mathrm{kpc}}} + 0.88\, e^{-\frac{(R-4.5\ \mathrm{kpc})^2-(R_\odot-4.5\ \mathrm{kpc})^2}{(2.9\ \mathrm{kpc})^2}}\right] \left(\frac{R}{R_\odot}\right)^{-1.65} e^{-\frac{|Z|}{H_h(R)}} , \quad (5)$$

with

$$H_h(R) = (1.5\ \mathrm{kpc}) \left(\frac{R}{R_\odot}\right)^{1.65} ,$$

and $R_\odot = 8.5$ kpc being the IAU recommended value of the Galactocentric radius at the Sun.

The space-averaged total interstellar mass density is obtained by summing the partial densities contributed by the different media:

$$\rho_0 = 1.36\, m_P\ (n_m + n_c + n_w + n_i + n_h) , \quad (6)$$

where m_P is the proton rest mass and the factor 1.36 accounts for the 9% by number of helium. The Z-dependence of ρ_0 is plotted in Fig. 1a at three different Galactic radii: $R = 5$ kpc (dotted line), $R = R_\odot$ (solid line), and $R = 12$ kpc (dashed line). To give a better idea of how the interstellar mass is radially distributed, we also plotted, in Fig. 1b, the R-dependence of the total column density of interstellar hydrogen nuclei through the Galactic disk, $N_0 = \int (n_m + n_c + n_w + n_i + n_h)\ dZ$.

The space-averaged interstellar thermal pressure can be written as a sum over the four true ISM phases (which do not include the molecular gas):

$$P_g = 1.09\, n_c\, kT_c + 1.09\, n_w\, kT_w + 2.09\, n_i\, kT_i + 2.27\, n_h\, kT_h , \quad (7)$$

where k is Boltzmann's constant, T_c, T_w, T_i, T_h are the temperatures, assumed to be uniform with the standard values $T_c = 80$ K, $T_w = T_i = 8000$ K and $T_h = 10^6$ K, and the numerical factors include the helium abundance and the ionization fractions given above.

The space-averaged interstellar turbulent pressure arising from random bulk motions is

$$P_t = 1.36\, m_P\, (n_m\, v_{rms,m}^2 + n_c\, v_{rms,c}^2) \quad (8)$$

with the one-dimensional turbulent velocities in the molecular and cold neutral media equal to $v_{rms,m} = 4.5$ km s^{-1} and $v_{rms,c} = 6.9$ km s^{-1}.

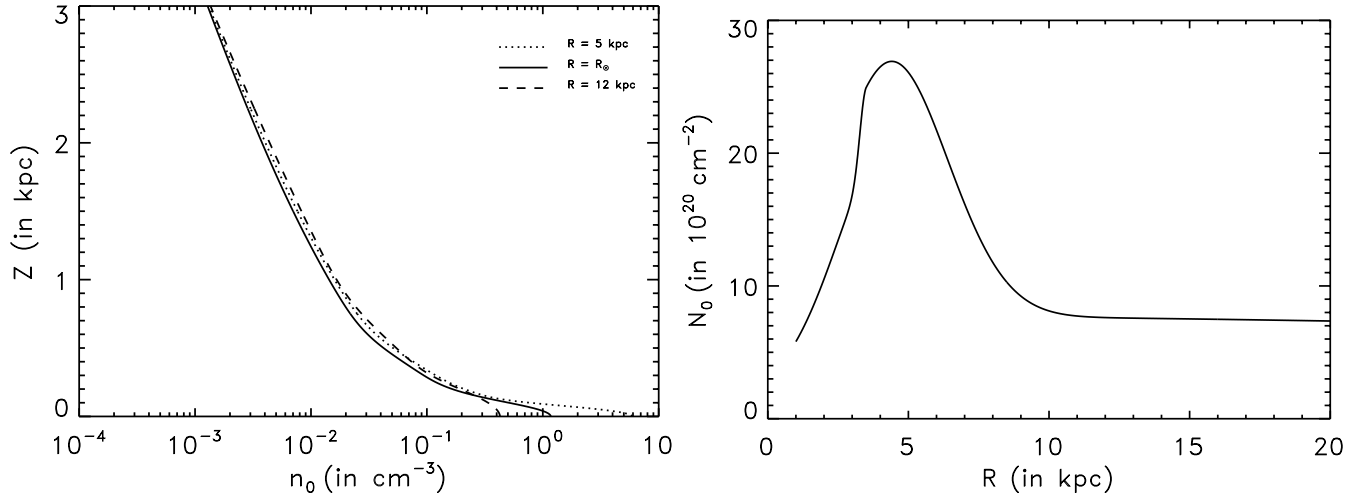

Fig. 1. a (left panel) Space-averaged number density of interstellar hydrogen nuclei as a function of Galactic height, at Galactic radii $R = 5$ kpc (dotted line), $R = R_\odot = 8.5$ kpc (solid line), and $R = 12$ kpc (dashed line). The space-averaged interstellar mass density is given by $\rho_0 = 1.36\, m_P\, n_0$ (see Eq. (6)). **b** (right panel) Total number of interstellar hydrogen nuclei per unit area on the Galactic disk, $N_0 \equiv \int n_0\, dZ$, as a function of Galactic radius.

The interstellar CR and magnetic pressures are

$$P_{CR}(R,Z) \;=\; \left(9.6\times10^{-13}\,\mathrm{ergs\,cm^{-3}}\right) \left[0.46\, e^{-\frac{R-R_\odot}{2.8\ \mathrm{kpc}}} \left(\mathrm{sech}\ \frac{Z}{255\ \mathrm{pc}}\right)^{n(R)} + 0.54\, e^{-\frac{R-R_\odot}{3.3\ \mathrm{kpc}}} \left(\mathrm{sech}\ \frac{Z}{255\ \mathrm{pc}}\right)^{b(R)}\right]^{\frac{1}{1.875}} \quad (9)$$

and

$$P_M(R,Z) \;=\; \left(10.3\times10^{-13}\,\mathrm{ergs\,cm^{-3}}\right) \left[0.46\, e^{-\frac{R-R_\odot}{2.8\ \mathrm{kpc}}} \left(\mathrm{sech}\ \frac{Z}{255\ \mathrm{pc}}\right)^{n(R)} + 0.54\, e^{-\frac{R-R_\odot}{3.3\ \mathrm{kpc}}} \left(\mathrm{sech}\ \frac{Z}{255\ \mathrm{pc}}\right)^{b(R)}\right]^{\frac{1}{1.875}}, \quad (10)$$

where the factor inside the brackets reflects the spatial dependence of the synchrotron emissivity, and the exponents $n(R)$ and $b(R)$ are given by the implicit equations

$$\int_0^\infty (\mathrm{sech}\ x)^{n(R)}\, dx \;=\; 0.617\, e^{\frac{R-R_\odot}{8.5\ \mathrm{kpc}}}$$

and

$$\int_0^\infty (\mathrm{sech}\ x)^{b(R)}\, dx \;=\; 6.0\, e^{\frac{R-R_\odot}{8.5\ \mathrm{kpc}}}\ ;$$

in particular, $n(R_\odot) = 4.60$, and $b(R_\odot) = 0.187$.

In Fig. 2, we show the space-averaged total interstellar pressure,

$$P_0 = P_g + P_t + P_{CR} + P_M\ , \quad (11)$$

at our three reference radii, and in Fig. 3, we show the average interstellar signal speed defined by

$$c_s = \sqrt{\frac{P_0}{\rho_0}}\ . \quad (12)$$

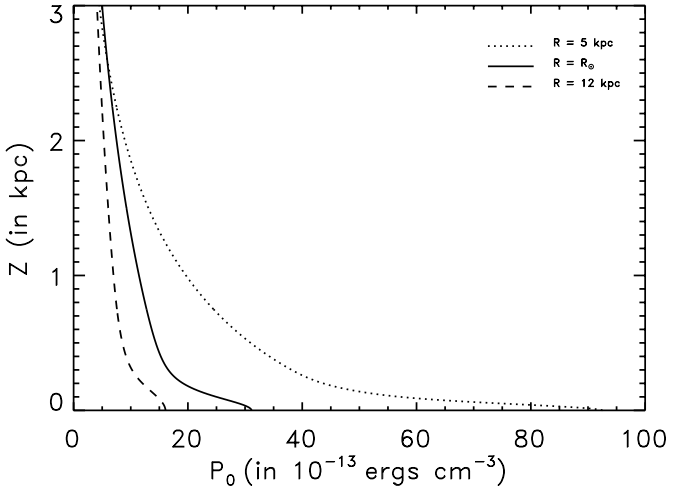

Fig. 2. Space-averaged interstellar pressure (Eq. (11)) as a function of Galactic height, at Galactic radii $R = 5$ kpc (dotted line), $R = R_\odot = 8.5$ kpc (solid line), and $R = 12$ kpc (dashed line).

Regarding the Galactic rotation curve, we assume that the rotation velocity, V, increases linearly from the center to $R = 3$ kpc, varies quadratically between 3 and 5 kpc, and remains equal to 220 km s^{-1} beyond 5 kpc. The corresponding rotation rate,

$$\Omega \equiv \frac{V}{R}\ , \quad (13)$$

and shear rate,

$$G \equiv R\, \frac{d\Omega}{dR}\ , \quad (14)$$

are displayed in Fig. 4 as a function of R.

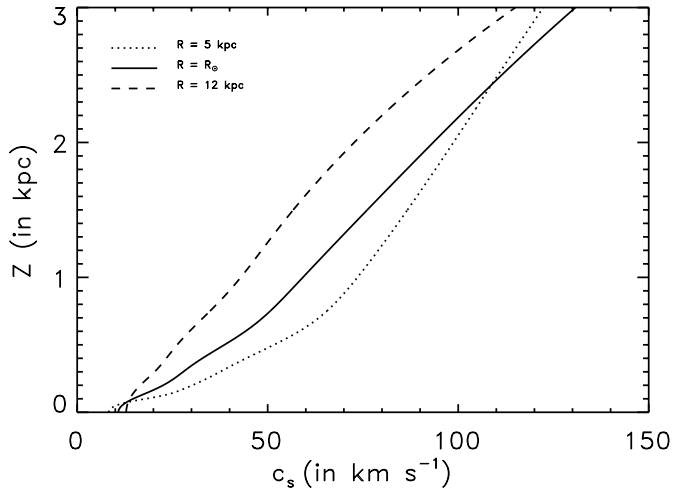

Fig. 3. Average interstellar signal speed (Eq. (12)) vs. Galactic height, at Galactic radii $R = 5$ kpc (dotted line), $R = R_\odot = 8.5$ kpc (solid line), and $R = 12$ kpc (dashed line).

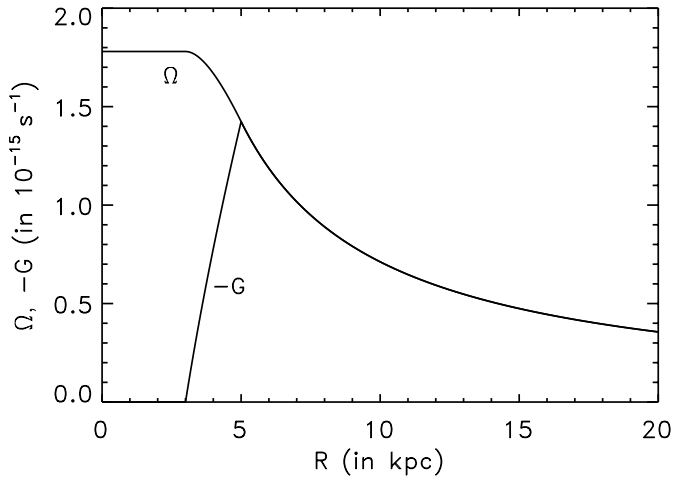

Fig. 4. Large-scale rotation rate, Ω (Eq. (13)), and minus the large-scale shear rate, $-G$ (Eq. (14)), against Galactic radius.

For the vertical component of the Galactic gravitational acceleration we take

$$-g_Z(R,Z) = (4.4\times10^{-9}\ \mathrm{cm\ s^{-2}})\, e^{-\frac{R-R_\odot}{4.9\ \mathrm{kpc}}}\, \frac{Z}{\sqrt{Z^2+(0.2\ \mathrm{kpc})^2}} + (1.7\times10^{-9}\ \mathrm{cm\ s^{-2}})\, \frac{R_\odot^2+(2.2\ \mathrm{kpc})^2}{R^2+(2.2\ \mathrm{kpc})^2}\, \left(\frac{Z}{1\ \mathrm{kpc}}\right) - 2\Omega(\Omega+G)Z\ . \quad (15)$$

With our adopted rotation law, the last term vanishes and we obtain the vertical profiles of Fig. 5.

The last important ingredient of the model is the SN distribution. Type Ia SNs (hereafter denoted by SNI) arise from old degenerate stars and have a rate per unit volume

$$\nu_I(R,Z) = (4.0\ \mathrm{kpc^{-3}\ Myr^{-1}})\, e^{-\frac{R-R_\odot}{4.9\ \mathrm{kpc}}}\, e^{-\frac{|Z|}{325\ \mathrm{pc}}}\ . \quad (16)$$

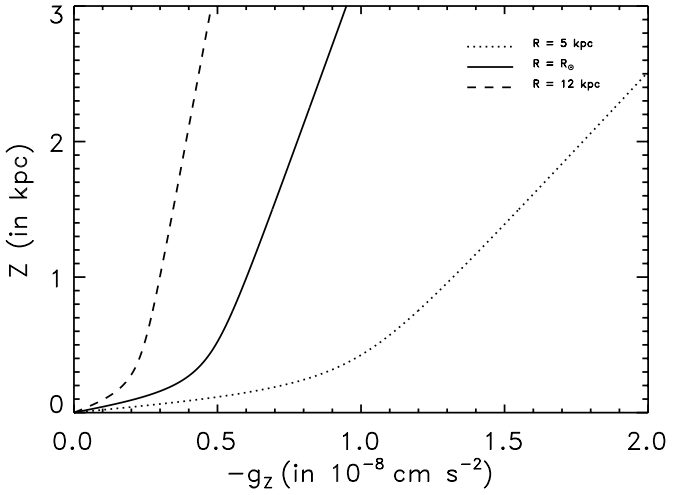

Fig. 5. Minus the vertical component of the Galactic gravitational acceleration (Eq. (15)) as a function of Galactic height, at Galactic radii $R = 5$ kpc (dotted line), $R = R_\odot = 8.5$ kpc (solid line), and $R = 12$ kpc (dashed line).

Type Ibc and Type II SNs (hereafter denoted by SNII) result from the core collapse of young massive stars. 40% of them are isolated and have a rate per unit volume

$$\nu_{II}(R,Z) = (14\ \mathrm{kpc^{-3}\ Myr^{-1}})\, e^{-\frac{(R-4.5\ \mathrm{kpc})^2-(R_\odot-4.5\ \mathrm{kpc})^2}{(2.9\ \mathrm{kpc})^2}}\, e^{-\frac{|Z|}{266\ \mathrm{pc}}}\ , \quad (17)$$

leading to a total isolated SN rate per unit volume

$$\nu_{SN}(R,Z) = \nu_I(R,Z) + \nu_{II}(R,Z)\ . \quad (18)$$

The other 60% are clustered and partake to the formation of SBs at a rate per unit volume

$$\nu_{SB}(R,Z) = (2.6\ \mathrm{kpc^{-3}\ Myr^{-1}})\, e^{-\frac{(R-4.5\ \mathrm{kpc})^2-(R_\odot-4.5\ \mathrm{kpc})^2}{(2.9\ \mathrm{kpc})^2}} \left(\frac{R}{R_\odot}\right)^{-0.58} e^{-\left(\frac{Z}{H_m(R)}\right)^2}\ , \quad (19)$$

where $H_m(R)$ is the molecular scale height, given below Eq. (1). The number, N, of SNs contributing to one SB varies between $N_{min} = 4$ and $N_{max} = 7230$, with an average of $\langle N\rangle = 30$, and is distributed according to

$$d\nu_{SB}(R,Z,N) = N_{min}\, \nu_{SB}(R,Z)\, \frac{dN}{N^2}\ . \quad (20)$$

Fig. 6a displays the vertical dependence of the SN and SB rates per unit volume at the three reference Galactic radii, while Fig. 6b gives the radial dependence of the corresponding rates per unit area, $\sigma_{SN}(R) \equiv \int \nu_{SN}(R,Z)\ dZ$, and $\sigma_{SB}(R) \equiv \int \nu_{SB}(R,Z)\ dZ$. The Galactic frequency of isolated SNs, obtained from an integration of Eq. (18) across the Galactic disk, is 1/(101 yr). For comparison, a spatial integration of Eq. (19) yields a SB frequency of 1/(2600 yr), corresponding to a clustered SN frequency of 1/(87 yr). Hence, it appears that isolated SNs are almost as frequent as their clustered counterparts.

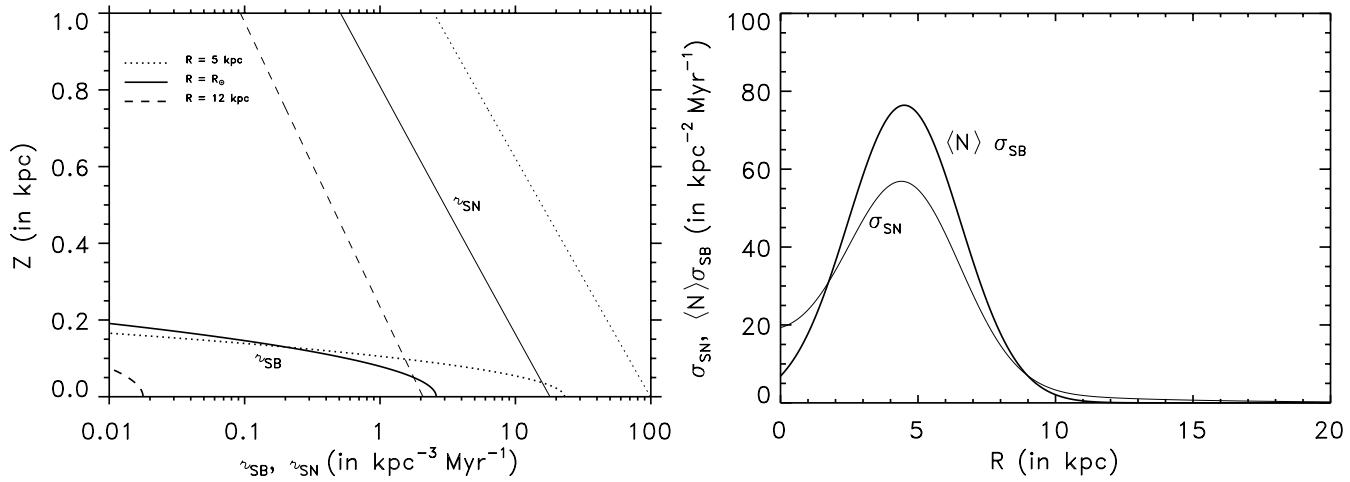

Fig. 6. a (left panel) Isolated SN rate per unit volume, r_{SN} (thin line; Eq. (18) together with Eqs. (16) and (17)), and SB rate per unit volume, r_{SB} (thick line; Eq. (19)), vs. Galactic height, at Galactic radii $R = 5$ kpc (dotted line), $R = R_\odot = 8.5$ kpc (solid line), and $R = 12$ kpc (dashed line). **b** (right panel) Isolated SN rate per unit area, $\sigma_{SN} \equiv \int \mathit{r}_{SN}\, dZ$ (thin line), and SB rate per unit area, $\sigma_{SB} \equiv \int \mathit{r}_{SB}\, dZ$, multiplied by $\langle N \rangle = 30$ (thick line), vs. Galactic radius. The SB rate was multiplied by the averaged number of clustered SNs per SB in order to yield the clustered SN rate, which can then be easily compared to the isolated SN rate.

3. Expansion of supernova remnants and superbubbles

We restrict our attention to the turbulent motions generated by isolated SNs and by SBs. Each of these events drives an outward propagating shock wave in the ISM, which sweeps up the ambient interstellar gas and magnetic field lines into an expanding cold dense shell. In this study, we make the thin-shell approximation whereby we let all the swept-up gas and field lines be concentrated at the leading shock wave.

In the case of isolated SNs, the energy input is instantaneous. For SNI, we adopt the standard value of 10^{51} ergs, while for SNII, we adopt the somewhat larger value of 1.14×10^{51} ergs, to account for the contribution from the wind blown by the progenitor star (see Ferrière 1995). In the case of SBs, the energy input is continuous, as it is due to repeated SN explosions and to stellar winds; its time dependence was calculated by Ferrière (1995) and is given by the luminosity curve plotted in Fig. 7.

The set of equations governing the expansion of the shell produced by an isolated SN or by a SB is presented in Ferrière (1995). This set includes evolution equations for the radius of the shell, for its mass and momentum per unit solid angle, and for the energy of the interior cavity. The momentum equations contain neither the magnetic tension force, which is negligible in the thin-shell approximation, nor the Coriolis force, which has a minor effect on the shell expansion (even though it is crucial for the alpha-effect). The external parameters (density, pressure...) entering the mass and momentum equations are taken from our model ISM (Eqs. (6), (11)...) at the Galactic radius of the explosion site. This approach is justified by (1) the result that the horizontal dimension of a cavity remains small compared to the radial scale length of the ISM parameters (see Sect. 5), and (2) the argument that interstellar magnetic fields keep the different ISM phases sufficiently tied together that the ISM can be treated as a homogeneous medium (Elmegreen 1992). In the framework

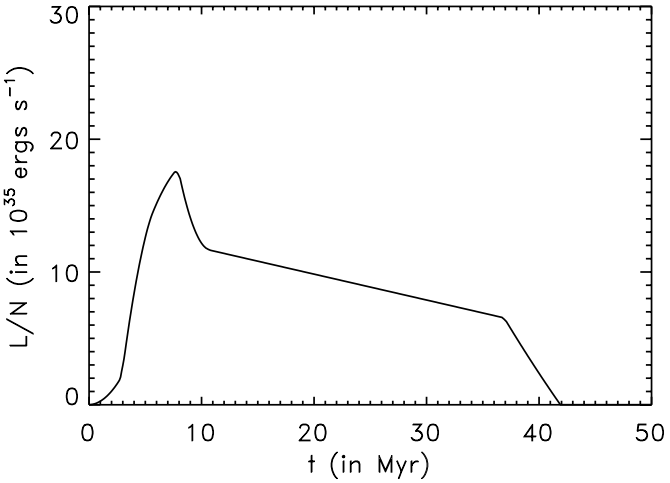

Fig. 7. SB luminosity per SN progenitor as a function of time.

of the above approximations, a shell is axisymmetric about the vertical, and its radius, mass, and velocity are functions of time, t, and polar angle, θ (defined with respect to a vertical axis through the SN or SB center), only.

A shell keeps expanding until its velocity (normal to itself) drops to 68% of the local external signal speed:

$$V_s = 0.68\, c_s \tag{21}$$

(the proportionality factor obtained by Ferrière [1995] was updated such as to remain consistent with the new ISM parameters). At that time, denoted by t_m, the shell merges with the background, and the swept field lines reconnect with the ambient magnetic field. For the following, it is important to bear in mind that t_m is a function of θ.

4. Dynamo parameters

The effect of a turbulent velocity field, $\mathbf{v}$, on the mean magnetic field, $\langle \mathbf{B} \rangle$, is described by the turbulent electromotive force,

$$\mathcal{E} = \langle \delta \mathbf{v} \times \mathbf{B} \rangle \ , \tag{22}$$

which is customarily expressed in terms of the alpha-tensor, α_{ij}, and the diffusivity tensor, β_{ijk}:

$$\mathcal{E}_i = \alpha_{ij} \langle B_j \rangle + \beta_{ijk} \frac{\partial \langle B_j \rangle}{\partial x_k} \tag{23}$$

(Moffatt 1978). Under the approximations introduced in Sect. 3, these tensors can be written in the form

$$\alpha_{ij} = \begin{pmatrix} \alpha_R & -V_{esc} & 0 \\ V_{esc} & \alpha_\Phi & 0 \\ 0 & 0 & \alpha_Z \end{pmatrix} \tag{24}$$

(Paper I) and

$$\beta_{ijk} \ = \ \beta_h \left(\in_{ijR} \ \delta_{kR} + \ \in_{ij\Phi} \ \delta_{k\Phi} \right) + \ \beta_v \ \in_{ijZ} \ \delta_{kZ} \tag{25}$$

(Paper II) in the Galactocentric cylindrical coordinate system (R, Φ, Z). Briefly, V_{esc} represents the effective vertical velocity at which the mean magnetic field is advected by turbulent motions; $\alpha_R, \ \alpha_\Phi$, and α_Z give the effective rotational velocity associated with the alpha-effect when $\langle \mathbf{B} \rangle$ is, respectively, radial, azimuthal, and vertical; β_h and β_v are the horizontal and vertical turbulent magnetic diffusivities; δ_{ij} is the unit tensor and $\in_{ijk}$ is the permutation tensor (equal to $+1, -1$, or 0, according to whether ijk forms an even permutation of $R\Phi Z$, an odd permutation of $R\Phi Z$, or neither).

In Papers I and II, we demonstrated that explosions occurring between Z_0 and $Z_0 + dZ_0$ with a rate per unit area $d\sigma$ give rise to the following contributions to the dynamo parameters:

$$dV_{esc} \ = \ \frac{1}{2} \, d\sigma \ S_m \ z \ , \tag{26}$$

$$d\alpha_\Phi \ = \ \frac{1}{2} \, d\sigma \ S_m \ z \ C_m \ \Omega \ t_m \ , \tag{27}$$

$$d\alpha_R \ = \ \frac{1}{2} \, d\sigma \ z \left\{ S_m \ C_m \ (\Omega + G) \ t_m - \int_0^{S_m} dS \ G \ t + \frac{1}{2} \ S_m \ G \ t_m \right\} , \tag{28}$$

$$d\alpha_Z \ = \ d\sigma \ \frac{1}{z} \ \left(\Omega + \frac{1}{2} G \right) \left\{ S_m \ C_m \ \varpi_m^2 \ t_m \ - \ \int_0^{S_m} dS \left(C + \frac{1}{4\eta} \right) \ \varpi^2 \ t \right\} \ , \tag{29}$$

$$d\beta_v \ = \ \frac{1}{6} \, d\sigma \ S_m \ z^2 \ , \tag{30}$$

$$d\beta_h \ = \ \frac{1}{6} \, d\sigma \ S_m \left(\frac{1}{2} \ \varpi_m \right)^2 \ , \tag{31}$$

at a vertical distance z above the explosion site. In the above expressions, ϖ is the horizontal radius of a shell a time t after the explosion; $S \equiv \pi \varpi^2$ is its horizontal cross-sectional area; $\eta \equiv \frac{t}{r_s} \frac{dr_s}{dt}$ is the instantaneous power law index for the evolution of the shell radius, r_s; C is the time-averaged value of $\frac{1}{2(1+2\eta)}$ up to the current time, t; and $\varpi_m, \ S_m, \ C_m$ are the values of $\varpi, \ S, \ C$ at the merge time, t_m. A detailed physical interpretation of Eqs. (26)−(31) is provided in Papers I and II and a summary is presented in Paper III.

The dynamo parameters in the Galactic disk are obtained by integrating Eqs. (26)−(31) over the observed SN and SB distributions, i.e., over

$$d\sigma \ = \ \left(r_{SN} + \int_{N_{min}}^{N_{max}} dr_{SB} \right) \ dZ_0 \ , \tag{32}$$

with r_{SN} and dr_{SB} given by Eqs. (18) and (20), respectively.

The numerical code used here to compute the dynamo parameters is an extension of the code written by Ferrière (1995) for the purpose of calculating the filling factor of hot cavities. It follows the temporal evolution of a large number of shells produced by isolated SNs and by SBs, with Z_0 and N spanning the observed range. It determines the merge time, t_m, and the maximum horizontal cross-sectional area, S_m, of each shell as well as the other quantities relevant to dynamo action (C_m and the integrals appearing in Eqs. (28) and (29)). The contributions from individual shells are then integrated over the SN/SB distribution given by Eq. (32). For a more detailed description of the numerical procedure, the interested reader is referred to Paper III.

5. Numerical results

We computed the non-vanishing components of the alpha- and diffusivity tensors (Eqs. (24) and (25)) at 15 equidistant Galactic radii ranging from 5 to 12 kpc. Inside 5 kpc, our model for the interstellar gas distribution becomes too uncertain and is no longer approximately plane-parallel. Beyond 12 kpc, the dynamo parameters have dropped to less than one hundredth of their maximum value. In Fig. 8, we display the results of the computation at R = 5, 7, 8.5, 10, and 12 kpc.

It clearly appears that the contribution from isolated SNs (thin line, visible only for α_Z) is everywhere negligible compared to that from SBs (thick line): isolated SNs give rise to less than 0.1% of the alpha-parameters and to less than 1% of the escape velocity and of the magnetic diffusivities. At first sight, this huge difference is somewhat surprising, given that isolated and clustered SNs have roughly the same Galactic frequency (see below Eq. (20)). However, as mentioned in Paper III, when N SNs are clustered together, the SB they create has a four-volume ($\int V \, dt$) which exceeds that of an individual SNR by a factor much larger than N. This is particularly true in a stratified medium, because the SBs that are luminous enough to push out of the dense gas layer are able to reach very large dimensions and live for a very long time, whereas most SNRs originate and remain confined to the vicinity of the midplane (Ferrière 1995).

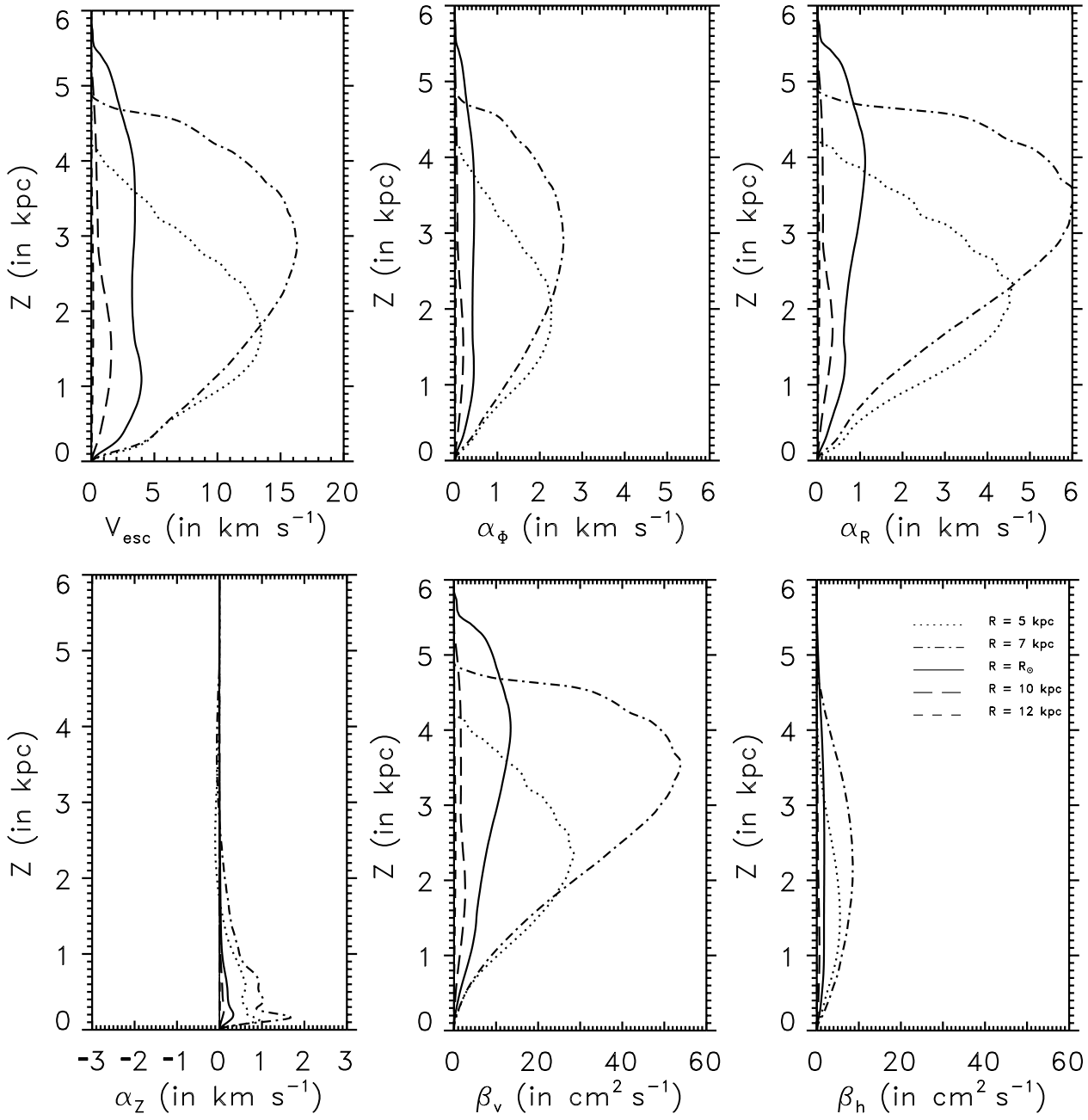

Fig. 8. Dynamo parameters due to SBs (thick line) and to isolated SNs (thin line, visible only for α_Z) as a function of Galactic height, at Galactic radii $R = 5$ kpc (dotted line), $R = 7$ kpc (dot-dashed line), $R = R_\odot = 8.5$ kpc (solid line), $R = 10$ kpc (long-dashed line), and $R = 12$ kpc (dashed line). V_{esc} is the effective vertical escape velocity (Eq. (26)); α_Φ, α_R, and α_Z are the effective rotational velocities associated with the azimuthal, radial, and vertical alpha-effects, respectively (Eqs. (27)−(29)); β_v and β_h are the vertical and horizontal magnetic diffusivities (Eqs. (30)−(31)).

In the case of the alpha-tensor, there exists another reason why clustering is favorable: when explosion centers are distributed along the vertical, high-Z explosions partially counteract the effect of low-Z explosions, thereby reducing the components of α. This reduction, which is significant for isolated SNs, becomes negligible for SBs whose scale height (see Eq. (19)) is small compared to the final size.

The curves relative to $R_\odot$ are similar in shape to those obtained in Paper III, but the overall magnitudes and characteristic scale heights are both smaller, mainly because a higher interstellar pressure was adopted in the present study.

The Z-dependence of the various dynamo parameters at $R_\odot$ was already examined and interpreted in Paper III. We briefly re-discuss it here from a slightly different point of view. For the purpose of the discussion, we focus on SBs and suppose that they all originate at the midplane. Accordingly, we replace z by Z in Eqs. (26)−(31) and drop the differentiation symbol d in $d\sigma$, dV_{esc}, $d\alpha_\Phi \ldots$ The escape velocity, V_{esc} (Eq. (26)),

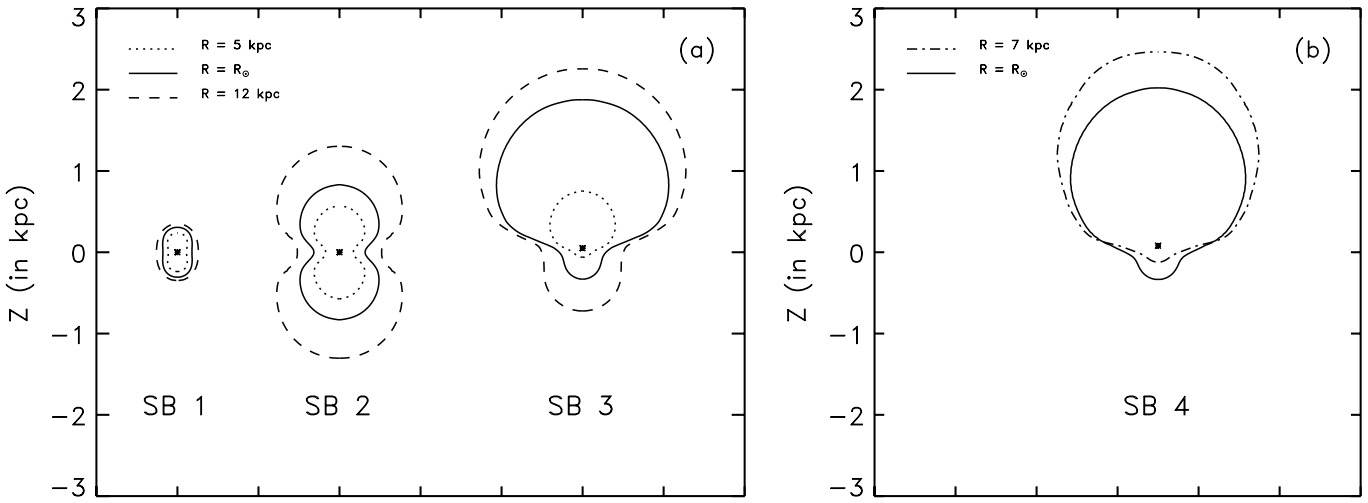

Fig. 9a and b. Shape of four representative SBs at the end of their expansion phase, the asterisk giving the position of the explosion center. SB 1 is produced by $N = \langle N \rangle = 30$ SNs and originates at the Galactic midplane ($Z_0 = 0$ pc); SB 2 has N = 300 and $Z_0 = 0$ pc; SB 3 has N = 300 and $Z_0 = 50$ pc; and SB 4 has N = 1000 and $Z_0 = 80$ pc. SBs in **a** are drawn at Galactic radii $R = 5$ kpc (dotted line), $R = R_\odot = 8.5$ kpc (solid line), and $R = 12$ kpc (dashed line), while the SB in **b** is drawn at $R = 7$ kpc (dot-dashed line) and $R = R_\odot$ (solid line). SB 1 merges in the time interval 11.0−11.9 Myr at 5 kpc, 13.0−13.9 Myr at $R_\odot$, and 15.6−16.9 Myr at 12 kpc. SB 2 merges in the time interval 12.3−12.7 Myr at 5 kpc, 17.2−17.4 Myr at $R_\odot$, and 23.8−31.4 Myr at 12 kpc. SB 3 merges in the time interval 10.9−12.8 Myr at 5 kpc, 15.6−30.2 Myr at $R_\odot$ and 23.1−43.0 Myr at 12 kpc. SB 4 merges in the time interval 13.7−26.0 Myr at 7 kpc and 17.3−22.8 Myr at $R_\odot$. Note that the same scaling is used along the horizontal and vertical axes.

at a given height Z is one-half the collision frequency with explosion shock waves ($\sigma\ S_m$) times the thickness of the magnetic layer pushed through that height by each explosion (Z). The azimuthal alpha-parameter, α_Φ (Eq. (27)), is proportional to the escape velocity times the angle by which the field lines swept by an explosion rotate under the effect of the Coriolis force ($\propto \Omega\ t_m$). The radial alpha-parameter, α_R (Eq. (28)), is also proportional to the escape velocity, but the angle by which the swept field lines rotate has a more complicated expression, which includes contributions from the Coriolis force ($\propto \Omega$) and from the large-scale shear ($\propto G$). The vertical alpha-parameter, α_Z (Eq. (29)), is proportional to the azimuthally-averaged effective large-scale rotation rate ($\Omega + \frac{1}{2}G$). The vertical and horizontal magnetic diffusivities, β_v (Eq. (30)) and β_h (Eq. (31)), are equal to one sixth of the collision frequency ($\sigma\ S_m$) times the square of the vertical and horizontal mean-free-paths (Z and $\frac{1}{2}\varpi_m$, respectively), as expected for three-dimensional diffusion coefficients.

If all SBs were cylindrical and merged in one go (i.e., S_m and t_m independent of Z), V_{esc}, α_Φ, and α_R would increase linearly with Z, α_Z would vanish, β_v would increase quadratically, and β_h would remain constant, up to the final height reached by the least powerful SBs, and above that height all functions would increase less rapidly due to the decreasing number of contributing SBs. In reality, only low- to average- luminosity SBs are approximately cylindrical (see, for example, SB 1 in Fig. 9a); high-luminosity SBs assume a more complicated shape as they tend to balloon out to large distances in the rarefied gas away from the midplane (see, for example, SB 2 in Fig. 9a). Likewise, SB lifetime usually increases upward, because our merging criterion (Eq. (21)), which is roughly equivalent to the condition $P_{int} = 1.46\ P_0$,[1] implies that SBs generally merge first at low Z, where the ambient interstellar pressure is strongest, and then at progressively higher Z. In consequence, the dynamo parameters in Fig. 8 (with the exception of α_Z) grow faster and turn over at a higher altitude than predicted for cylindrical SBs.

The behavior of the vertical alpha-parameter is a little more subtle. As explained in Paper III, the sign of α_Z is closely related to the shape of SBs. Consider, for instance, the SB displayed in Fig. 10, and suppose that the mean magnetic field, $\langle \mathbf{B} \rangle$, is uniform and oriented in the positive Z-direction. Then, according to Eqs. (23) and (24), α_Z is simply the Z-component of the turbulent electromotive force, $\langle \delta\mathbf{v} \times \mathbf{B} \rangle$, divided by the mean magnetic field's strength. The turbulent velocity responsible for the alpha-effect arises as the interstellar gas set into diverging motion by the explosion counterrotates with respect to the effective large-scale rotation rate, $\Omega + \frac{1}{2}G$, in an attempt to conserve its angular momentum, so it is essentially clockwise about the Z-axis. The magnetic field swept by the explosion follows the bubble's surface, and, therefore, points away from the Z-axis up to the height of maximum horizontal cross-section and toward the Z-axis thereabove. As a result, the considered SB gives a positive (negative) contribution to the Z-component of $\langle \delta\mathbf{v} \times \mathbf{B} \rangle$, and, hence, to α_Z, in regions where its horizontal cross-section increases (decreases) upward. Since most SBs tend to be pinched by the dense interstellar gas and elevated pressure near the midplane (see Fig. 9), α_Z is found positive at low $Z > 0$ and negative high above the plane.

[1] This condition results from the requirement of pressure balance across the shell ($P_{int} \simeq \rho_0 V_s^2 + P_0$) combined to the merging criterion (Eq. (21)) together with the definition of the interstellar signal speed (Eq. (12)).

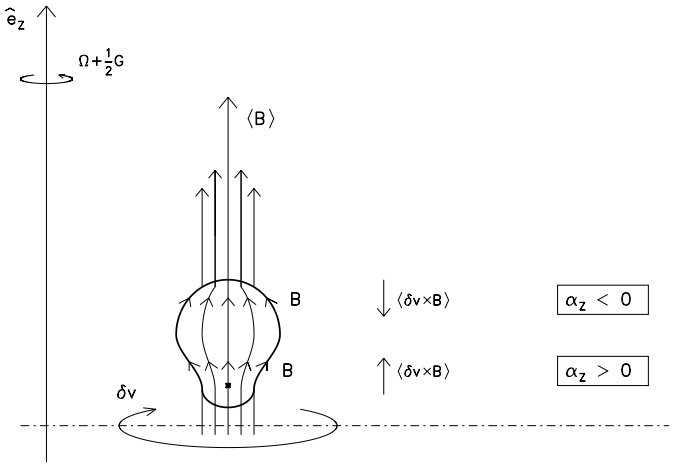

Fig. 10. Schematics explaining the sign of the vertical alpha-parameter, α_Z. The mean magnetic field, $\langle \mathbf{B} \rangle$, is in the positive Z-direction. A SB originating somewhat above midplane (at the position indicated by the asterisk) produces an asymmetric elongated shell (thick line). The turbulent velocity responsible for the alpha-effect, $\delta \mathbf{v}$, is opposite to the effective large-scale rotation rate, $(\Omega + \frac{1}{2} G)$. Magnetic field lines swept by the SB are deformed along the shell. Below (above) the height of maximum horizontal cross-section, the turbulent electromotive force, $\langle \delta \mathbf{v} \times \mathbf{B} \rangle$, has a positive (negative) Z-component, so that α_Z is positive (negative).

We now turn to the R-dependence. The vertical profiles of the dynamo parameters in Fig. 8 remain qualitatively the same throughout the radial range of our computation. Their typical values vary little between 5 and 8 kpc, and they fall off rapidly beyond the solar circle, though not as rapidly as the SB rate per unit area (Fig. 6b). This relatively weak radial dependence arises because the steep drop in the SB rate is counteracted by an outward decline in the interstellar pressure (Fig. 2) and column density (Fig. 1b), which allows most SBs to live longer and reach greater dimensions at larger Galactic radii (see Fig. 9a).

On the other hand, there exist a few particularly luminous off-center SBs (like SB 4 in Fig. 9b) which are so severely affected by the gas density stratification that they actually grow higher at smaller radii. After bursting through the dense gas layer, these SBs find it easier to expand upward at smaller R, where they encounter less resistance from the ambient density (see Fig. 1a). Moreover, after their equatorial region merges and lets the interior pressure equilibrate with the external ambient pressure, the net driving pressure force on their upper portions is stronger at smaller R, thereby pushing their polar cap to higher altitudes. The existence of powerful SBs with very different behaviors regarding the vertical expansion explains why the vertical profiles of the dynamo parameters cannot be characterized by a single scale height which varies monotonically with Galactic radius.

To close up this section, we provide contour plots of the dynamo parameters in Fig. 11. Because of the limited radial range of our computation, we had to extrapolate the numerical results presented above. Inside $R = 5$ kpc, we opted to take the functions obtained at 5 kpc and simply weight them by the factor $\sigma_{SB}(R)\ e^{\frac{R}{3\ \mathrm{kpc}}}$, where σ_{SB} is the SB rate per unit area (Fig. 6b) and the exponential factor is meant to account for the increase in interstellar pressure toward the Galactic center. Outside $R = 12$ kpc, all functions have become so small that the exact extrapolation procedure has no impact on the contour plots.

Broadly speaking, the dynamo parameters peak at $R \simeq 7$ kpc and (except for α_Z) $|Z| \simeq 2.5 - 3.5$ kpc. The fact that the peak in dynamo activity occurs farther out than the peak in SB rate (see Fig. 6b) is a direct consequence of the longer lifetime and larger volume reached by SBs at greater R (see Fig. 9a). The peak values are $V_{esc} \simeq 16\ \mathrm{km\ s^{-1}}$, $\alpha_\Phi \simeq 2.6\ \mathrm{km\ s^{-1}}$, $\alpha_R \simeq 6.0\,\mathrm{km\ s^{-1}}$, $\alpha_Z \simeq 1.7\,\mathrm{km\ s^{-1}}$, $\beta_v \simeq 54 \times 10^{26}\ \mathrm{cm^2\ s^{-1}}$, and $\beta_h \simeq 9 \times 10^{26}\ \mathrm{cm^2\ s^{-1}}$, about half an order of magnitude larger than the maximum values reached at the solar circle.

The standard Galactic dynamo operates through a combination between the large-scale differential rotation and the alpha-effect. The strength of these two processes against magnetic diffusion can be measured by the dimensionless numbers

$$C_G = \frac{|G|\ h^2}{\beta} \tag{33}$$

and

$$C_\alpha = \frac{\alpha\ h}{\beta}\ , \tag{34}$$

respectively, and their combined strength is given by the dynamo number,

$$D = C_G\, C_\alpha = \frac{|G|\ \alpha\ h^3}{\beta^2}\ . \tag{35}$$

With $h = Z$, $\alpha = \alpha_\Phi$, and $\beta = \beta_v$ (appropriate for a disk geometry), the dynamo number works out to be $D \simeq 8$ in the peak region. This is a comfortable value, large enough to guarantee dynamo action (when $V_{esc} = 0$) and small enough to exclude very high dynamo modes. When $V_{esc} \neq 0$, dynamo action also requires that the ratio $\frac{V_{esc}}{\alpha_\Phi}$ be less than a critical value ~ 8 (Schultz, Elstner, & Rüdiger 1994); this condition, too, is fulfilled in the peak region, where we find $\frac{V_{esc}}{\alpha_\Phi} \simeq 6$.

Two more conclusions can be drawn from the values of the ratio $\frac{C_\alpha}{C_G}$ in the peak region. First, for $\alpha = \alpha_\Phi$, this ratio yields the magnetic pitch angle, p, defined as the angle between the large-scale magnetic field and the azimuthal direction, via $\tan p \simeq -\sqrt{\frac{C_\alpha}{C_G}}$. Here, we have $\frac{C_\alpha}{C_G} \simeq 0.03$, leading to a pitch angle $p \simeq 10°$, which lies at the lower end of the observational range (Beck et al. 1996). Second, for $\alpha = \alpha_R$, the ratio $\frac{C_\alpha}{C_G}$ quantifies the relative importance of the radial alpha-effect compared to the large-scale shear in the production of large-scale azimuthal magnetic field. The relatively high value $\simeq 0.07$ obtained here indicates that the Galactic dynamo is of the $\alpha^2\Omega$-type, rather than the commonly assumed $\alpha\Omega$-type.

6. Discussion

In this paper, we computed the dynamo parameters, i.e., the non-vanishing components of the tensors α and β, which describe

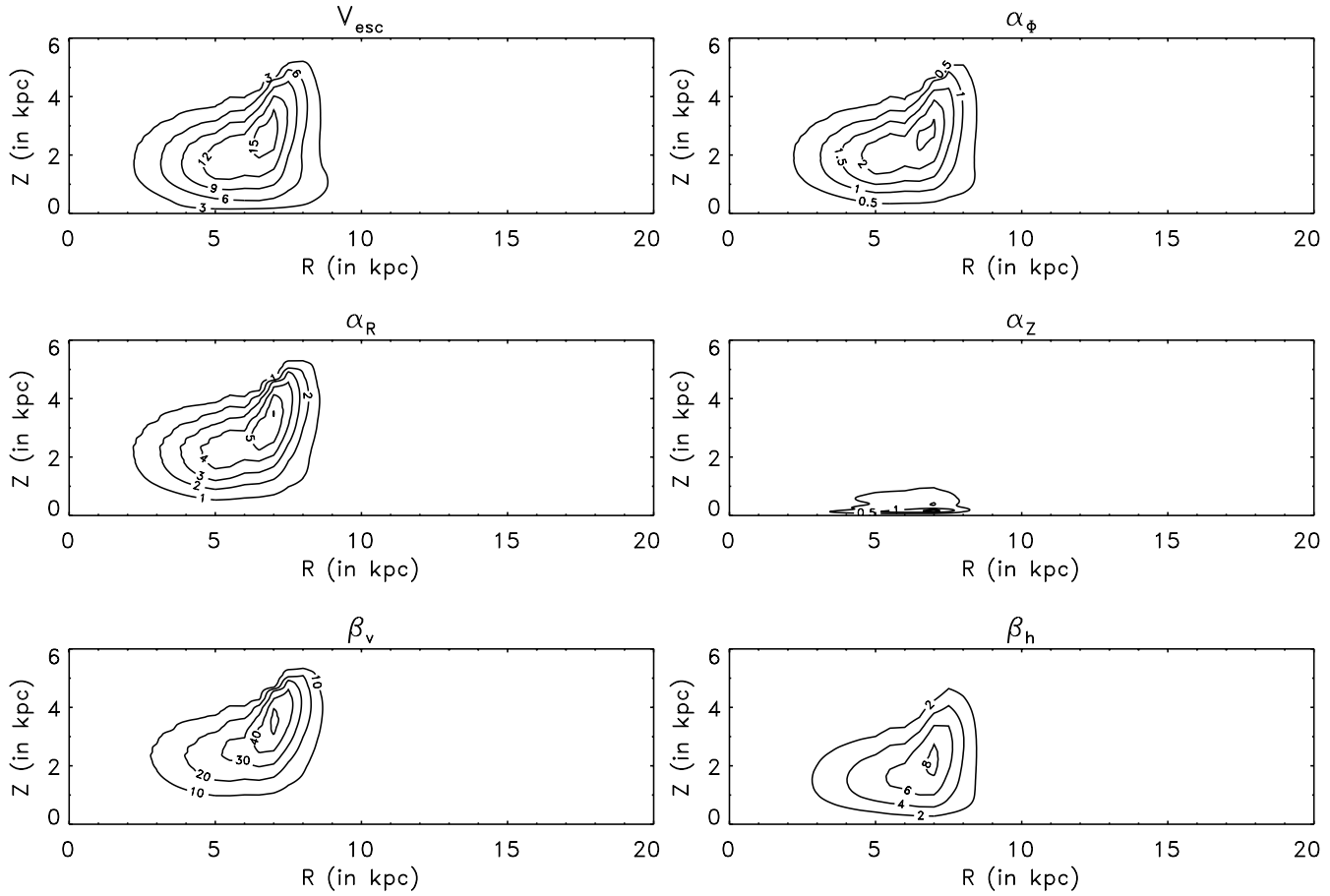

Fig. 11. Contour plots of the dynamo parameters in a given meridional plane. V_{esc} is the effective vertical escape velocity (Eq. (26)); α_Φ, α_R, and α_Z are the effective rotational velocities associated with the azimuthal, radial, and vertical alpha-effects, respectively (Eqs. (27)−(29)); β_v and β_h are the vertical and horizontal magnetic diffusivities (Eqs. (30)−(31)). Velocities are in km s^{-1} and magnetic diffusivities are in units of 10^{26} cm^2 s^{-1}.

the effects of turbulent motions on the large-scale Galactic magnetic field. We considered only the turbulent motions directly driven by SN explosions, ignoring those associated with the contraction phase of SNRs and SBs as well as those produced by a totally different mechanism. As argued in Papers I and II, turbulent motions other than those considered here probably have a limited impact on the α-parameters, α_Φ, α_R, α_Z, whereas they are likely to reduce the escape velocity, V_{esc}, and to enhance the magnetic diffusivities, β_v and β_h.

The numerical results are displayed in the form of vertical profiles at 5 different Galactic radii (Fig. 8) and in the form of contour plots (Fig. 11). The dynamo parameters appear to be almost entirely due to clustered SNs, even though these are hardly more frequent than their isolated counterparts. They peak in a double ring located at $R \simeq 7$ kpc and $Z \sim \pm 3$ kpc. In this double ring, the dynamo number (Eq. (35)) is sufficiently high and the ratio $\frac{V_{esc}}{\alpha_\Phi}$ sufficiently low to allow for magnetic field amplification.

Contrary to earlier studies which found $\alpha_Z < 0$ above midplane (based on a second-order correlation approximation (Rüdiger & Kichatinov 1993) or on a fully numerical simulation of individual SN explosions (Kaisig, Rüdiger, & Yorke 1993)), we obtain $\alpha_Z > 0$ up to $Z \gtrsim 2$ kpc. This new result can be attributed to the "peanut" or "pear" shape of most SBs in the strongly stratified ISM. Together with the confirmation that $\alpha_\Phi > 0$ above midplane, it may have important implications for the solutions of the dynamo equation, in particular for the existence of nonaxisymmetric solutions (see Rüdiger, Elstner, & Schultz 1992).

Our results are evidently affected by uncertainties in the input ISM parameters and by working approximations. The former are reviewed and extensively discussed in Ferrière (1995) and Ferrière (1998). The latter, which concern either the modelling of a shell's dynamic behavior (thin-shell approximation, merging criterion. . .) or the analytical formulae employed for the dynamo parameters (Eqs. (26)−(31)), are discussed in Ferrière (1995) and in Papers I and II, respectively.

Because of the many sources of error, the overall amplitude of the computed dynamo parameters could easily be off by a factor of 2 or 3. Likewise, their exact spatial dependence should not be taken too seriously, especially at high altitudes where the ISM parameters become increasingly uncertain and dynamo action arises solely from a small number of particularly powerful SBs whose characteristics are not well established. The most

uncertain parameter is undoubtedly α_Z, which turns out to be highly dependent upon the exact shape of expanding shells, with the consequence that not only its characteristic amplitude but also its very sign are still questionable.

Furthermore, our axisymmetric study is unable to provide any information on the longitudinal structure of α and β. Since our model ISM is described by the azimuthally-averaged values of the ISM parameters, it is implicitly expected to lead to the azimuthally-averaged α and β. However, owing to the numerous nonlinearities in the problem, this is not strictly the case. On the other hand, the longitudinal variation of α and β is probably weaker than that of other ISM parameters. For instance, the explosion rate varies significantly between spiral arms and interarm regions, but an increase in the explosion rate is usually accompanied by an increase in the interstellar pressure, which entails a decrease in the size and lifetime of individual bubbles, so that ultimately α and β vary only moderately with longitude. Because of this self-regulatory effect, the values obtained numerically are, in fact, likely to be reasonably close to the true azimuthally-averaged values.

Finally, the results presented in this paper are based on the present-day structure of the ISM. If introduced as such into the dynamo equation, they make it possible to predict whether SN-driven turbulence is, at the present time, able to maintain the large-scale magnetic field, $\mathbf{B}_0$, but they do not permit a complete determination of the exact history of $\mathbf{B}_0$. The reason is that the dynamo parameters themselves evolve in the course of time.

In most dynamo calculations, the temporal dependence of α and β is usually presumed to arise only from a dependence on $\mathbf{B}_0(t)$ and it is embodied in a quenching factor of the form

$$\frac{1}{1+\left(\frac{B_0(t)}{B_{sat}}\right)^n}\ , \tag{36}$$

which decreases with increasing magnetic field strength.

In the case at hand, an increase in B_0 does, indeed, lead to a decrease in the components of α and β, primarily through an enhancement of the background pressure and signal speed, which slows down the expansion of SBs and forces them to merge earlier (see Eq. (21)), and secondarily through a higher magnetic tension in the swept field lines, which opposes SB expansion perpendicular to $\mathbf{B}_0$. However, the quenching effect can not be described by such a simplistic law as Eq. (36), because
(1) The final size and lifetime of individual SBs, and, hence, their contributions to α and β, depend in a complicated manner on the external magnetic pressure (which appears both in the momentum equations and in the merging criterion).
(2) The quenching mechanism due to magnetic tension in the swept field lines is inherently anisotropic.
(3) The dynamo parameters at a given Galactic location depend not only on $\mathbf{B}_0$ at that location, but also on the whole profile of $\mathbf{B}_0$ throughout the domain of influence of SBs reaching the considered location.
Moreover, $\mathbf{B}_0$ is not the only time-dependent ISM parameter that affects α and β. The SN rate, the gas density and pressure, the characteristic interstellar scale heights, the gravitational field, the rotation rate... are all likely to have evolved since the Galaxy's formation, in ways not entirely independent of the magnetic field's own evolution.

A rough estimation of the temporal evolution of the large-scale magnetic field can, nevertheless, be obtained from the dynamo equation by using our dynamo parameters weighted by a factor of the form shown in Eq. (36) with, say, $n = 2$ and B_{sat} equal to the equipartition magnetic field (e.g., Brandenburg et al. 1993).

Note that some authors have criticized the use of Eq. (36), arguing that dynamo action does, in fact, saturate long before the large-scale magnetic field builds up to equipartition (e.g., Vainshtein & Cattaneo 1992; Kulsrud & Anderson 1992). Their argument is based on the notion that the dynamo requires the formation of turbulent magnetic structures down to the very small diffusive scales at which field lines can reconnect; the field strength at these diffusive scales, they claim, exceeds the large-scale field strength by a huge factor (greater than the square root of the magnetic Reynolds number), and the process of magnetic field amplification by the dynamo saturates as soon as the magnetic field at the small diffusive scales reaches equipartition, i.e., when the large-scale field is still far below equipartition.

However, the kind of turbulence envisioned by Vainshtein & Cattaneo (1992) is very different from the SN-driven turbulence considered here. While the former gives rise to a smooth magnetic energy spectrum increasing toward large wavenumbers, the latter is more likely to produce two widely separated magnetic energy peaks with comparable amplitude, namely, a first peak at the large scales characteristic of SNR and SB shells, and a second peak at the small diffusive scales presumably generated upon merging (for instance, following collision with an interstellar cloud) and allowing the swept field lines to reconnect with the background magnetic field. The resulting spectrum would be similar to that associated with the stretch-twist-fold mechanism (Vainshtein & Zel'dovich 1972), which, Vainshtein & Cattaneo (1992) themselves recognize, avoids their general criticism. We, therefore, believe that a Galactic dynamo founded on the action of SN explosions and SBs is able to amplify the large-scale magnetic field to equipartition and subsequently maintain it at that level.

References

Beck R., Brandenburg A., Moss D., Shukurov A., Sokoloff D., 1996, ARA&A, 34, 155
Brandenburg A., Donner K., Moss D., Shukurov A., Sokoloff D., Tuominen I., 1993, A&A, 271, 36
Elmegreen B.G., 1992, The Galactic Interstellar Medium, ed. D. Pfenniger & P. Barthodi (Berlin: Springer-Verlag), p157
Ferrière K.M., 1993a, ApJ, 404, 162 (Paper I)
Ferrière K.M., 1993b, ApJ, 409, 248 (Paper II)
Ferrière K.M., 1995, ApJ, 441, 281
Ferrière K.M., 1996, A&A, 310, 438 (Paper III)
Ferrière K.M., 1998, ApJ, 497, 759
Fich M., Blitz L., Stark A.A., 1989, ApJ, 342, 272
Kaisig M., Rüdiger G., Yorke H.W., 1993, A&A, 274, 757
Kulsrud R.M., Anderson S.W., 1992, ApJ, 396, 606

Mc Cray R., Snow T.P., Jr., 1979, ARA&A, 17, 213
Moffatt H.K., 1978, Magnetic Field Generation in Electrically Conducting Fluids (Cambridge: Cambridge Univ. Press)
Parker E.N., 1971, ApJ, 163, 255
Rüdiger G., Elstner D., Schultz M., 1992, The Cosmic Dynamo, IAU Symposium 157, ed. F. Krause, K.-H. Rädler, & G. Rüdiger (Kluwer Academic Publishers), p321
Rüdiger G., Kichatinov L.L., 1993, A&A, 269, 581
Schultz M., Elstner D., Rüdiger G., 1994, A&A, 286, 72
Steenbeck M., Krause F., Rädler K.-H., 1966, Z. Nat., A21, 369
Vainshtein S.I., Cattaneo F., 1992, ApJ, 393, 165
Vainshtein S.I., Ruzmaikin A.A., 1971, AZh., 48, 902; English trans. Soviet Astron., 15, 714 (1972)
Vainshtein S.I., Zel'dovich, Ya.B., 1972, Sov. Phys. – Uspekhi. 15, 159